KIM – A method to estimate the relative density of calcareous sands

Franz Tschuchnigg
Institute of Soil Mechanics and Foundation Engineering and Computational Geotechnics / University of Technology, Graz, Austria,
franz.tschuchnigg@tugraz.at

Marco Hofer
Institute of Soil Mechanics and Foundation Engineering and Computational Geotechnics / University of Technology, Graz, Austria,
marco.hofer@student.tugraz.at

ABSTRACT: This paper describes the challenges that arise during quality control of deep vibro-compaction works on land reclamation projects. The aim of deep vibro-compaction is to densify the fill to a certain relative density I_D, which can be measured indirectly by performing Cone Penetration Tests (CPT). Due to the fact, that carbonate sands show significantly lower q_c-values than silica sands under the same conditions well established empirical correlation methods between the cone resistance q_c and the relative density I_D, which are mostly based on the results obtained from silica sands, cannot be used for carbonate sands. Therefore, the Karlsruhe Interpretation Method (KIM) is applied as correlation method within this paper. The KIM consists of numerical analyses of the spherical cavity expansion (SCE) problem and the empirical results of calibration chamber tests. This paper focuses on the FE model to solve the spherical cavity expansion problem using both, a hypoplastic and an elasto-plastic constitutive soil model. The paper investigates additionally the sensitivity of soil parameters on the results of a spherical cavity expansion analysis and comprises a model verification, where computed results are compared with closed form solutions. In addition, the hypoplastic soil parameter calibration tool ExCalibre is discussed and finally, the automation of the whole KIM process is presented. The results of the paper clearly show, that the KIM, in combination with the proposed FE model, is a very powerful tool, which is able to accommodate the intrinsic characteristics of calcareous sand.

Keywords: spherical cavity expansion; KIM; hypoplasticity; ExCalibre

1. Introduction

The quality control of deep vibro-compaction works is an important contractual issue, which is often defined in technical terms such as the relative density I_D. The density of an already compacted soil can be indirectly determined by means of cone penetration tests (CPT) and applying appropriate correlation methods between the received cone resistance q_c and the relative density I_D. The most commonly used interpretation methods such as correlations according to Schmertmann [1] or Baldi [2], are derived from series of calibration chamber tests based on a wide range of different silica sands and are therefore not capable to reproduce the characteristics of carbonate sands [3]. As an alternative to these correlation methods, the KIM (Karlsruhe Interpretation Method) has the advantage of considering the behavior of calcareous sands [4].

In the first part of the paper the influence of the carbonate content on the soil properties is briefly presented, followed by a short overview regarding the Karslruhe Interpretation Method. The third (main) part focuses on the solution of the spherical cavity expansion problem, consisting of a verification of the finite element model and the application of different constitutive models. The numerical studies of the SCE investigate additionally the influence of the dilatancy angle ψ and the initial stress state. After that the hypoplastic soil parameter calibration tool ExCalibre [5] is discussed and further a full KIM analysis is presented. Finally, the automation of the KIM using Python scripting is schematically outlined.

2. Influence of the carbonate content on soil properties

Calcareous sands show a significantly higher tendency towards grain crushing than silica sands. This is related to the fact, that $CaCO_3$ is classified by Mohs` scale of mineral hardness only by a value of roughly three, whereas silica sand reaches a value of approximately seven. Hence, the influence of the carbonate content on soil properties has to be taken into account, when correlating q_c values (obtained from CPT tests) to relative densities I_D.

Based on detailed laboratory investigations on 11 soil samples with different $CaCO_3$ content, Tschuchnigg et al. [3] stated, that especially four geotechnical parameters, namely the limit void ratios e_{min} and e_{max}, the critical friction angle φ'_c and the grain density ρ_s are increasing with increasing carbonate content of sand.

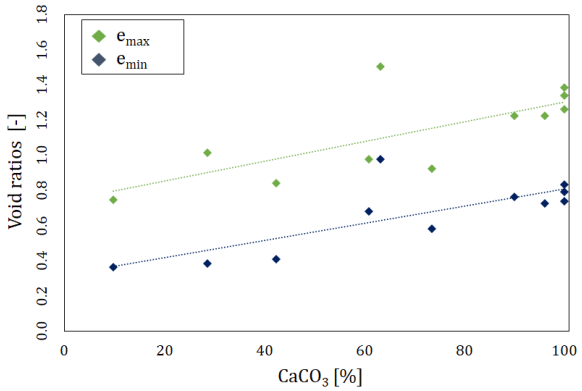

Figure 1. Influence of carbonate content on limit void ratios e_{max} and e_{min} [6]

The impact of the cabonate content (of a calcareous sand) on the limit void ratios is examplary shown in Fig. 1. A higher carbonate content results in higher limit void ratios, which further has an influence on the soil's unit weight γ and consequently on the mean effective stress p_0'. Hence, with an increase of $CaCO_3$, γ and p_0' decrease, which finally leads to lower cone resistances q_c.

3. Karlsruhe Interpretation Method

The Karlsruhe Interpretation Method (KIM) is a semi-empirical method to correlate the cone resistance q_c with the relative density I_D. This method was originaly developed by Cudmani [7]. The key components of the KIM are on the one hand numerical solutions of the spherical cavity expansion (SCE) problem and on the other hand empirically determined shape factors k_q. The KIM, as developed by Cudmani [7], uses the hypoplastic soil model according to Von Wolffersdorff [8]. More recently Meier [9] applied the KIM to investigate calcareous sands and showed, that the method is capable to represent the complex material behaviour of calcareous sand, thus to compute realistic values of q_c.

The final KIM equation is given as follows:

$$q_c = k_q(I_D) * p_{LS}(p_0, I_D) \tag{1}$$

The empirical part of the KIM, namely the shape factor k_q was established by Cudmani [7]. On the basis of calibration chamber tests the shape factor k_q can be expressed with Eq. (2). As a result of the performed tests Cudmani [7] concluded, that the shape factor (k_q) only depends on the relative density I_D.

$$k_q = \left(1.5 + \frac{5.8 * {I_D}^2}{{I_D}^2 + 0.11}\right) \tag{2}$$

The numerical part (second part of the KIM – see Eq. (1)) is related to the calculation of the limit pressure (p_{LS}) obtained from the solution of the spherical cavity expansion problem, where p_{LS} depends on the effective mean pressure p_0' and the relative density I_D.

The limit pressure p_{LS} can be determined finally with Eq. (3). Therefore, the KIM parameters a_i and b_i are necessary, which can be obtained from a curve fitting procedure as described in Cudmani [7] or Winkler [10].

$$p_{LS} = a * {p'_o}^b \tag{3}$$

$$a = a_1 + \frac{a_2}{a_3 + I_D} \tag{4}$$

$$b = b_1 + \frac{b_2}{b_3 + I_D} \tag{5}$$

The following chapters present some details of the finite element model, which is used to solve the SCE problem.

4. Spherical cavity expansion

In general, the cavity expansion in soils is considered as a one-dimensional boundary problem, which consists of a spherical cavity with an initial radius a_0. In the used finite element model the cavity is modelled inside a continuum (soil) and initially the entire model (continuum plus cavity) is loaded with the mean effective pressure p_0'. During the simulation of the spherical cavity expansion the radius (a) of the cavity is increased by applying volumetric strains inside the cavity. With ongoing expansion the cavity pressure increases, approaching a certain limit value denoted as the limit pressure p_{LS} [7, 10]. This resulting limit pressure p_{LS} is one of the main parts of the Karlsruhe Interpretation Method (see Eq. (1)).

The SCE was already studied by Cudmani and Osinov [11], where they used a finite difference code and the hypoplastic soil model according to Von Wolffersdorff [8] to solve the problem. Tschuchnigg and Winkler [4] modeled the SCE problem of the spherical cavity expansion with the finite element software PLAXIS 2D [12] to enable the possibility of applying different soil models and to investigate the influence of soil parameters and the initial stress field on p_{LS}.

The details of the FE model and the utilized numerical settings are given in Tschuchnigg and Winkler [4] and Winkler [10]. However, the necessity of averaging the SCE results is outlined in the following and some investigations related to the calculation phases are presented.

4.1. Averaging process

Preliminary studies performed by Winkler [10] showed that the flow rule (when using elasto-plastic constitutive models) has a significant influence on the results of the FEA. Different to the application of an associated flow rule causes the application of a non-associated flow rule a slightly non-uniform deformation behavior of the cavity. However, Winkler [10] already showed, that averaging the received pressure-expansion curves delivers satisfying results compared with the closed-form solution presented by Yu and Houlsby [13].

The arrangement of the the nodes (A to I) and stress points (K to T) of the finite element model, which are used for the averaging procedure, are shown in Fig. 2.

To visualize the resulting pressure expansion curves, principle effective stresses σ_1' are plotted against the normalized deformations (a/a_0) of the sphere. The results of the spherical cavity expansion (as exemplary illustrated in Fig. 3) show the stresses (σ_1') for each stress point (K to T) as a consequence of the normalized deformations a/a_0 of the related nodes (A to I).

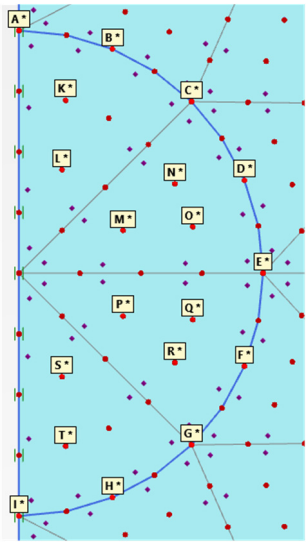

Figure 2. Selected nodes and stress points

The studies to investigate the averaging procedure of the SCE results were performed with material set MC 3 of Table 1. The results showed (when using the MC 3 material with a non-associated flow rule) high scattering of the pressure expansion curves of the output nodes and stress points. Wheras applying an associated flow rule with $\psi = 30\,°$ results in a uniform deformation behavior of all nodes and stress points. Hence, when applying a non-associated flow rule, an averaging process is required. The resulting averaged $\sigma_1' - a/a_0$ curve and the computed results from the different pairs of nodes and stress points (e.g. A & K) can be seen in Fig. 3.

Based on numerical investigations Winkler [10] further suggested to exclude the results of the southern- and northern-most selected nodes (A and I) and stress points (K and T). This approach could be confirmed by comparing the averaged $\sigma_1' - a/a_0$ curves using all nodes and stress points and the averaged solution, where the nodes (A and I) and the stress points (K and T) are neglected, with the results of the closed-form solution of Yu and Houlsby [13] (see Fig. 4).

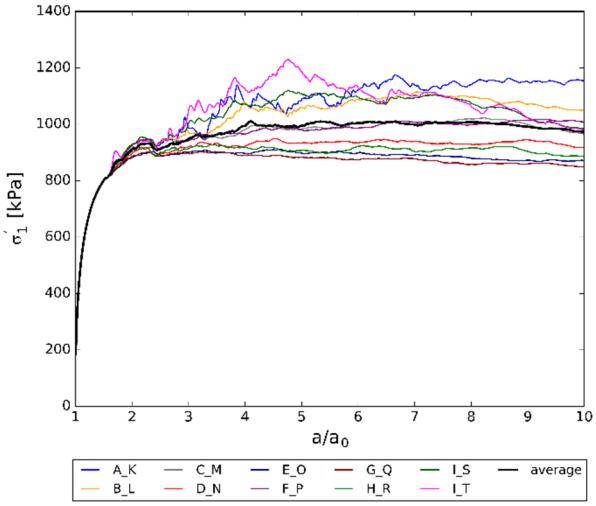

Figure 3. Pressure-expansion curves for all output nodes and stress points including the averaged solution (MC 3 material set and non-associated flow rule with $\psi = 0\,°$)

4.2. Calculation phases

In the following the influence of the calculation procedure (different volumetric strains applied inside the cavity) on the resulting limit pressure, applying different soil models, materials and initial stress situations, is investigated. One example is shown in Fig. 5, where the pressure-expansion curves, using the Hardening Soil (HS) [14] model, for various applied volumetric strains are plotted.

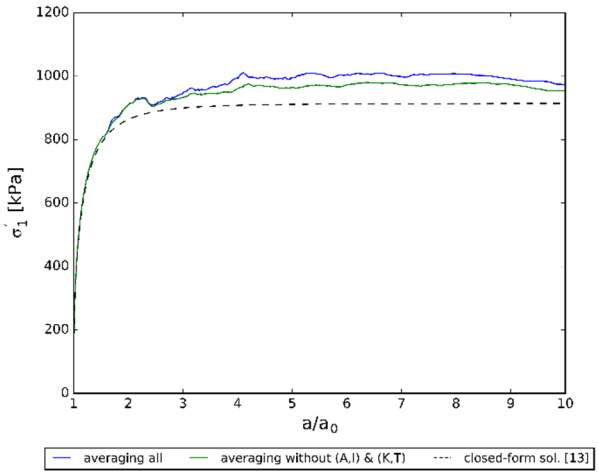

Figure 4. Average approaches and closed-form solution [13] (MC 3 material set and non-associated flow rule with $\psi = 0\,°$)

The used input parameters for the FEA are also given in Fig. 5. In the first analysis, phase one and two are defined with a volumetric strain of 500% followed by 200% for phase three and four. Whereas in the other FEA, all phases are calculated with identical volumetric strains of 200%, 300% and 400% respectively. Fig. 5 clearly shows, that there is almost no difference between the curves. The same results can be observed for the linear elastic – perfectly plastic Mohr-Coulomb model (MC) and the hypoplastic soil model. Thus, it can be concluded that the numerical model is very robust. Based on the studies it is recommended to apply volumetric strains between 300% and 400% for each calcuation phase.

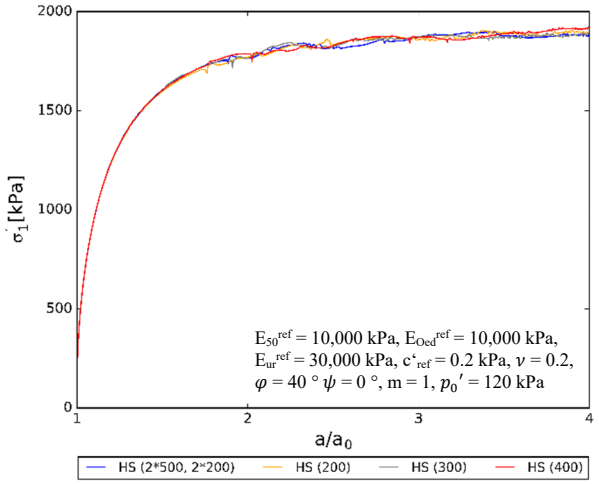

Figure 5. Pressure-expansion curves (HS soil model) for different calculation procedures (applied volumetric strains)

Table 1. Material sets for MC model

Material	E [kPa]	φ' [°]	ψ [°]	K_0 [-]	p_0' [kPa]
MC 1	5000	20	[0, 20]	1.0	120
MC 2	10000	42	[0, 5, 12, 17]	1.0	120
MC 3	25000	30	[0, 30]	[0.5, 1.0]	50

4.3. Model verification

To validate the finite element model the analytical solution of Yu and Houlsby [13] is used. This closed-form solution allows to consider different magnitudes of the dilatancy angle, thus accounts for non-asscociated plasticity. The following chapter shows the influence of the dilatancy angle on the resulting pressure-expansion curves for different soil models. Additionally, the influence of the lateral earth pressure coefficient K_0 on p_{LS} is investigated.

4.3.1. Mohr-Coulomb model

For the calculations with the MC soil model (linear elastic – perfectly plastic soil model), the three different material sets given in Table 1 are used. For all material sets an effective cohesion of $c' = 0$ kPa and a Poisson's ratio of $\nu = 0.2$ were defined.

The results of the materials sets MC 1 and MC 2 (presented in Fig. 6 and Fig. 7) show a very good agreement with the closed-form solution, although the pressure-expansion curves using a non-associated flow rule show a small amount of scattering. Fig. 7 confirms the impact of non-associated plasticity and indicates that the resulting $\sigma_1' - a/a_0$ curves get smoother with an increase of the dilatancy angle. The solution for the non-associated material with $\psi = 0$ presented in Fig. 6 is already very smooth, which is caused by the relatively low amount of non-associativity ($\varphi' - \psi$) of material set MC 1.

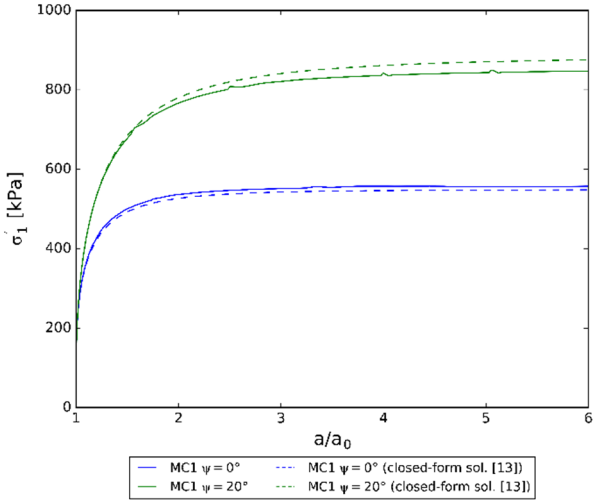

Figure 6. Pressure-expansion curves: MC 1 material set and different dilatancy angles ψ

Additional studies have been performed to investigate the effect of the initial stress field on p_{LS}. In the FE model the initial stress field is generally generated by means of a surcharge layer, while the unit weight of the continuum ($\gamma_{continuum}$) is set to zero (see Fig. 10). To investigate the impact of a non-isotorpic initial stress state the finite element analyses using material set MC 3 were repeated with a K_0-value according to Jaky [15] ($K_0 = 1 - sin\varphi'$). Fig. 8 represents the contour plots of total displacements $|u|$ when assuming an associated flow rule and different K_0-values. This figure indicates, that applying an associated flow rule results in an almost uniform deformation behavior for both lateral earth pressure coefficients ($K_0 = 1.0$ and $K_0 = 0.5$).

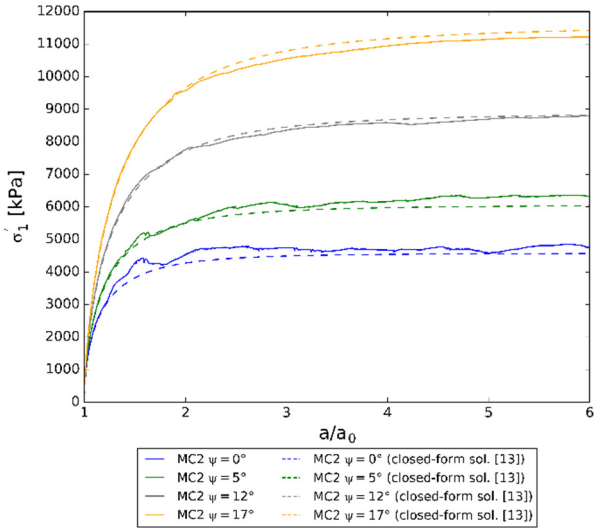

Figure 7. Pressure-expansion curves: MC 2 material set and different dilatancy angles ψ

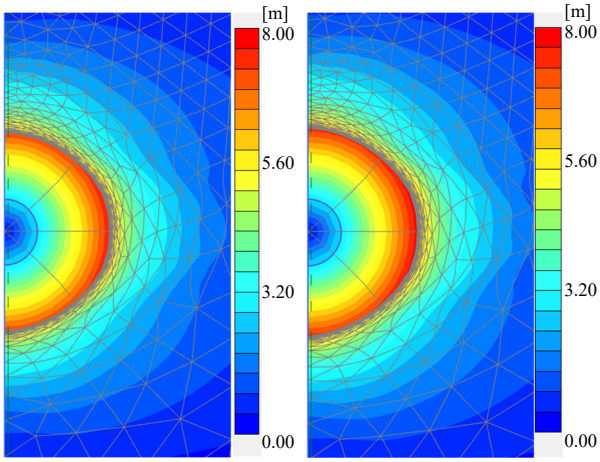

Figure 8. Total displacements: MC 3 material set; $\psi = 30$ ° and different K_0-values ($K_0 = 1.0$ left and $K_0 = 0.5$ right)

To enable a comparison between the different K_0-values with respect to p_{LS} the models with $K_0 = 0.5$ were solved with different unit weights of the surcharge layer. Once the unit weight was defined with the same value as for the FEA with $K_0 = 1.0$ to model the situation with the same σ_v'. In another FEA the unit weight of the surcharge layer was increased, to model the situation where initial mean effective pressure p_0' is the same as in the case

Table 2. Input parameters HS model

Material	E_{50}^{ref} [MPa]	E_{ur}^{ref} [MPa]	E_{Oed}^{ref} [MPa]	φ' [°]	ψ [°]	K_0 [-]
HS	50	150	50	40	10	[0.357, 1.0]

$K_0 = 1.0$. The stress situation within the continuum for $K_0 = 1.0$ (using a unit weight of the continuum of $\gamma = 0\ kN/m^3$) and applying only a unit weight for the surcharge layer ($\gamma_{surcharge}$) can be seen in Fig. 10.

Fig. 9 represents the pressure-expansion curves for the three described situations using a non-associated flow rule ($\psi = 0$) and an associated flow rule with $\psi = 30$ °. One can see that the limit pressures increase with increasing K_0-values (as expected). From Fig. 9 it can also be seen that the difference between the pressure-expansion curves applying $K_0 = 1.0$ and $K_0 = 0.5$ with the same initial mean effective pressure p_0' are relatively small, wheras the differences between the results for $K_0 = 1.0$ and $K_0 = 0.5$ with the same vertical effective pressure σ_v' are significantly larger. Similar observations are obtained with an associated flow rule. However, when using associated plasticity the pressure-expansion curves tend to increase further, eventhough large strains are applied to the model. In other words, a horizontal tangent and a well defined limit pressure is not achieved in these analyses.

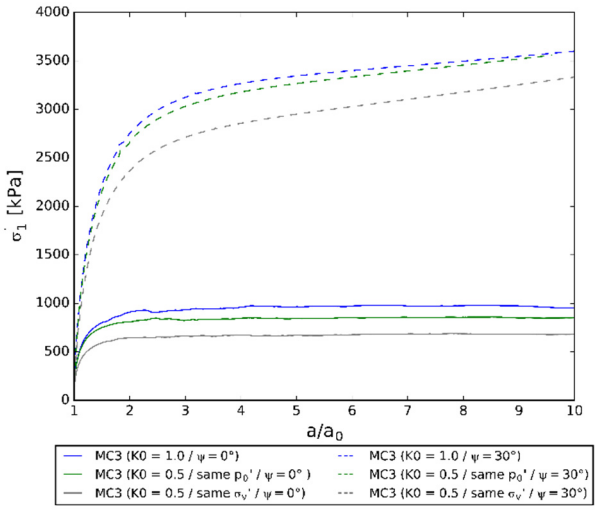

Figure 9. Pressure-expansion curves for material set MC 3 (associated and non-associated flow rule) with different K_0 values and different initial stress conditions

4.3.2. Hardening Soil model

This chapter investigates the influence of the initial stress field when using the Hardening Soil model. So far the initial stresses were generated by activating a surcharge layer with a certain unit weight γ combined with a unit weight of $\gamma = 0$ kN/m³ for the continuum (see Fig. 10). For the following investigations (additionally to the case with $K_0 = 1.0$) a non-uniform initial stress state was defined. For theses FEA the surcharge layer was deactivated and the continuum was modelled with a non-zero unit weight. The finite element analyses using a K_0 value of 0.357 are defined once with the same initial mean effective pressure p_0' (as in the FEA with $K_0 = 1.0$) at the center of the cavity and once with the same effective vertical pressure σ_v' (as discussed in chapter 4.3.1.) at the center of the cavity. A schematical represenation of the non-uniform initial stress field with the same value of σ_v' is shown in Fig. 10.

The used parameter set includes an effective cohesion $c' = 0.2$ kPa and a Poisson's ratio of $\nu = 0.2$. The void ratios e_{min}, e_{max} and e_{init} were defined as 0.49, 0.78 and 0.50 respectively. The remaining stiffness and strength parameters are given in Table 2 and the results of the studies are plotted in Fig. 12.

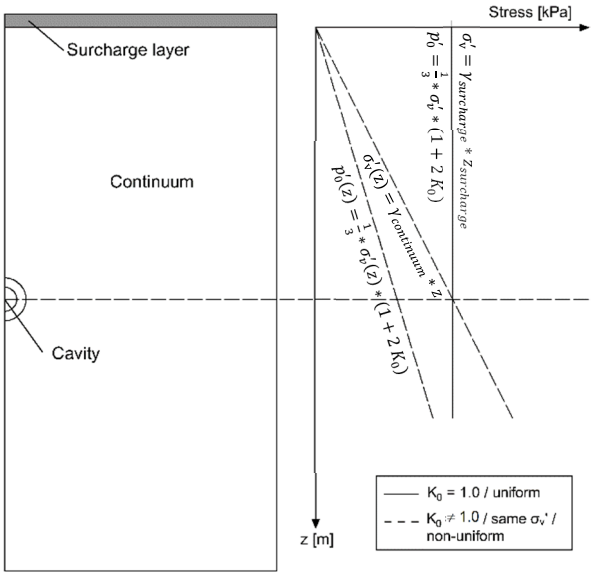

Figure 10. Representation of different initial stress fields: $K_0 = 1.0$ and non-uniform stress field ($K_0 \neq 1.0$ and same σ_v')

Numerical studies confirmed that the problem of the continuous increase of p_{LS} during the SCE process (see FEA with associated plasticity in Fig. 9) can be controlled by using a dilatancy-cut-off, as available in the HS model. This option sets the mobilised dilatancy angle ψ_m to zero at the point where the maximum void ratio e_{max} (which is an input parameter) is reached. But it has to be mentioned, that the change of void ratio e is related to the change of volumetric strain ε_v (see Eq. (6)). A schematical representation of the dilatancy-cut-off can be seen in Fig. 11 [12].

$$-(\varepsilon_v - \varepsilon_v^{init}) = ln\left(\frac{1-e}{1+e_{init}}\right) \tag{6}$$

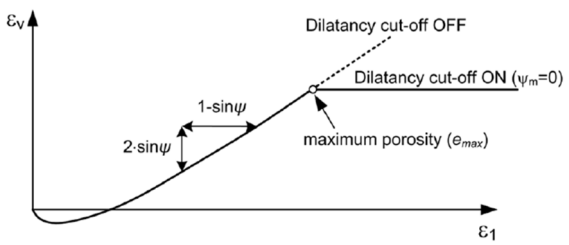

Figure 11. Dilatancy-cut-off principle of the HS model ([12], [16])

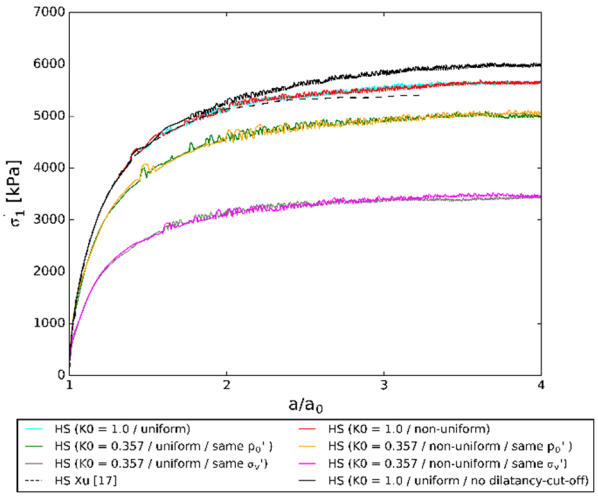

Figure 12. Pressure-expansion curves with different K_0-values and different initial stress conditions (Hardening Soil model)

Fig. 12 shows clearly that there is almost no difference between the application of a uniform stress state and a non-uniform stress state (where the continuum is modeled with a non-zero unit weight, without the requirement of a surcharge layer). Fig. 12 also shows that the obtained results for $K_0 = 1.0$ show a very good agreement with the results presented by Xu [17], who used a K_0 value of 1.0. Similar studies have been performed for seven other material sets found in literature [17], where all FEA showed the same tendencies. Based on that it can be concluded again, that the difference between the pressure-expansion curves for $K_0 = 1.0$ and $K_0 = 0.357$ with the same initial mean effective pressure p_0' are smaller than the differences between the results for $K_0 = 1.0$ and $K_0 = 0.357$ with the same initial vertical effective pressure σ_v'. Further it can be seen that the dilatancy-cut-off causes the resulting pressure-expansion curves to become horizontal at large values of a/a_0. Hence, a clear limit pressure is computed.

5. Hardening Soil model vs hypoplastic soil model

In this chapter the spherical cavity expansion was modelled with optimized HS-parameters (based on a parameter set for the hypoplastic model). The aim of this study is to investigate the performance of an elasto-plastic constitutive model compared to hypoplasticity (since the originally developed Karlsruhe Interpretation Method uses the hypoplastic soil model). For these investigations a material set found in literature [18] was used. The Hardening Soil as well as the hypoplastic (HP) soil parameters can be found in Table 3 and Table 4.

The stiffness parameters of the HS model for the loose Hostun sand were, compared to the parameters given in [18] slightly adjusted to $E_{Oed}^{ref} = E_{50}^{ref}$ and $E_{ur}^{ref} = 3 * E_{50}^{ref}$. For the different parameter sets triaxial tests, applying a confining pressure of $\sigma_3' = 100$ kPa, were modelled with the PLAXIS Soil Test Tool. Finally the obtained results were compared with the results given in [18], as shown in Fig. 13. The computed stress-strain curves of the triaxial compression test show a very good agreement with both, the laboratory test results and the numerical results presented by Marcher et al. [18].

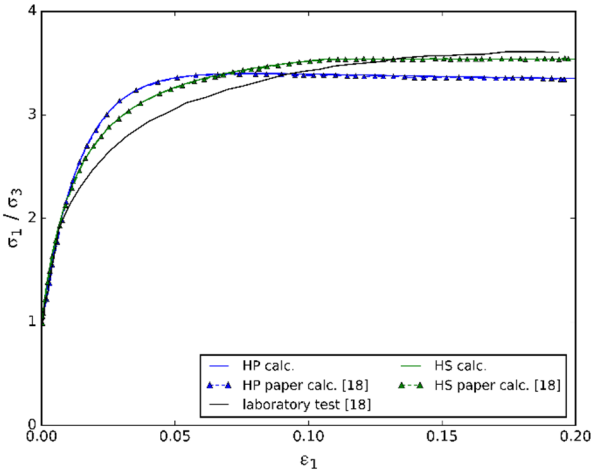

Figure 13. Triaxial test on loose Hostun sand (confining pressure $\sigma_3' = 100$ kPa)

For the HS model the dilatancy-cut-off option was selected, but due to the fact that the limit void ratios, e_{min} and e_{max} were not explicitly given in [18], the hypoplastic parameter set was used to calculate the limit void ratio e_{max} (using Eq. (10)).

The computed pressure-expansion curves for the two density states and the different constitutive soil models are illustrated in Fig. 14. This figure shows that the Hardening Soil model calculates very similar results, thus similar limit pressures. However, a closer look indicates that for the loose material the difference between the applied constitutive soil models is less than for the dense material. Based on the performed numerical studies it can be concluded, that the Hardening Soil model is also able to provide satisfying results, but, due to the fact that this constitutive soil model does not take pyknotropy into account, for each density state a new Hardening Soil parameter set has to be generated. Thus, it is associated with high effort. The hypoplastic soil model on the other hand has the advantage, that it takes the influence of density (pyknotropy) into account.

Table 3. Hardening Soil parameters – Hostun sand

Material	E_{50}^{ref} [MPa]	E_{Oed}^{ref} [MPa]	E_{ur}^{ref} [MPa]	φ' [°]	ψ [°]	m [-]
Dense sand	30	28	90	44	14	0.55
Loose sand	12	12	36	34	0	0.75

Table 4. Hypoplastic soil parameters – Hostun sand

Material	φ_c [°]	h_s [MPa]	n [-]	e_{d0} [-]	e_{c0} [-]	e_{i0} [-]	α [-]	β [-]
Dense & loose sand	32	1000	0.29	0.61	0.91	1.09	0.19	2

Fig. 15 shows exemplary results of performed FEA to analyse the SCE problem using the hypoplastic soil model according to Von Wolffersdorff [8]. This figure illustrates the change of void ratio e with the pressure p' during the application of volumetric strains.

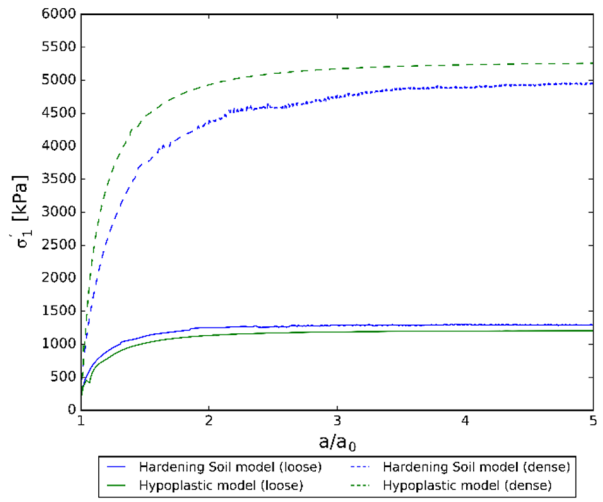

Figure 14. Pressure-expansion curves for loose and dense Hostun sand with the Hardening Soil and the hypoplastic soil model

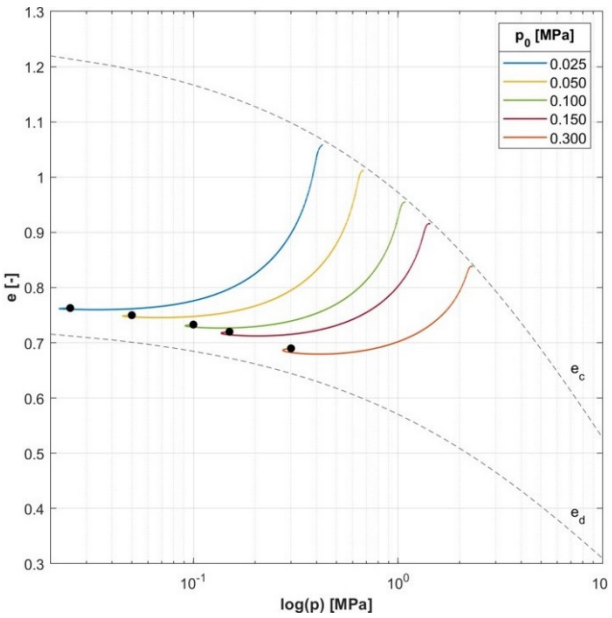

Figure 15. FEA of the SCE problem: log(p') – e – diagram using a hypoplastic soil model (relative density I_D = 0.9) [10]

6. ExCalibre

The advantage of the hypoplastic soil model for the KIM was discussed in chapter 5. In the following the utilization of the automatic calibration tool ExCalibre [5] is investigated. With ExCalibre users have the possibility to calibrate input parameters for advanced constitutive soil models, such as the hypoplastic sand model according to Von Wolffersdorff [8]. A model-specific calibration algorithm is used to achieve a reliable set of parameters. To perform the calibration the user has to provide the following data as input:

- Specific gravity, angle of repose, sieve-passings
- Lab data of oedometric compression tests
- Lab data of triaxial compression tests

For the automatic calibration of the hypoplastic parameters, the laboratory tests given in [6] were used as input for ExCalibre. These studies include two oedometric compression tests, one on a loose and one on a dense soil sample. Furthermore four triaxial compression tests are used, again two for loose and two for dense soil samples with different confining pressures.

Preliminary studies related to ExCalibre (performed by Winkler [10]) already indicated the influence of the number and the type of laboratory tests (provided to the ExCalibre input file) on the resulting hypoplastic parameters. Therefore, different combinations of the laboratory test results have been used as ExCalibre input files. Table 5 summarizes the different input sets. For every input set in ExCalibre a hypoplastic parameter set was calibrated. The differences of the calibrated parameters, compared to the hypoplastic parameters in [6] are exemplary shown in Fig. 16 (for h_s, α, β and e_0). The hypoplastic parameter set published in [6] is further denoted as "Set 0" and was taken as reference, since the intention of this study was to compare a standard ("experience-based") parameter determination with the automatic procedure as used by ExCalibre.

Fig. 16 indicates, that the h_s parameter shows big deviations for the input sets where only one dense oedometric compression test was used. This result was expected, since h_s should be obtained from oedometric compression tests on initially very loose specimens.

Table 5. Different input sets for the calibration tool ExCalibre

Input set	Oed 1 (dense)	Oed 2 (loose)	Triax 100 (dense)	Triax 100 (loose)	Triax 600 (dense)	Triax 600 (loose)
1	x	x	x	x	x	x
2		x	x		x	
3	x			x		x
4	x	x	x		x	
5	x	x	x			x
6	x	x		x	x	
7	x			x	x	
8		x		x	x	

Table 6. Hypoplastic parameters for "Set 0" and input "Set 4"

Material	φ_c [°]	h_s [MPa]	n [-]	e_{d0} [-]	e_{c0} [-]	e_{i0} [-]	α [-]	β [-]
Set 0 acc. to [6]	36.3	39.00	0.525	0.740	1.261	1.450	0.05	1.97
ExCalibre 4	34.2	35.72	0.452	0.607	1.215	1.458	0.30	2.00
|Δ| [%]	5.8	8.4	13.9	18.0	3.7	0.6	500.0	1.5

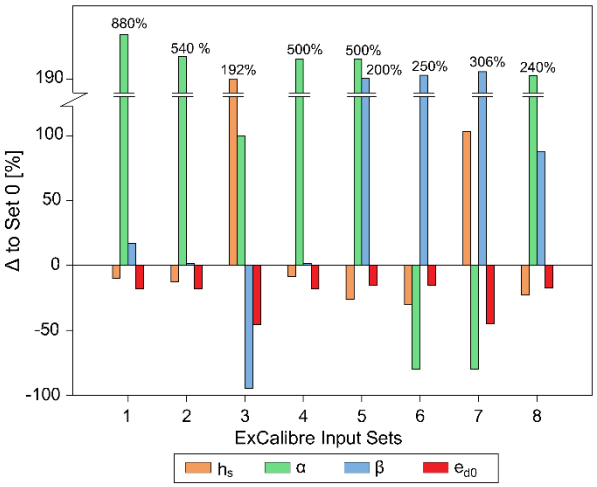

Figure 16. Differences between "Set 0" [6] and ExCalibre results (for h_s, α, β and e_{d0})

The parameter α can generally be calibrated by performing drained triaxial tests on initially dense samples. ExCalibre input set 7 and 8 include triaxial test data of dense samples, but show a significant difference for the parameter α. These results indicate that the calibration of α is highly effected by the number and type of data used as an input for ExCalibre. Further, it can be concluded that the input sets one, two and four show very high deviations for α coupled with only small deviations for all other hypoplastic parameters.The reason for such high deviations of α is not clear at the moment. Differently, the limit void ratio e_{d0} shows only significant deviations for input set 3 and 7, which include only one dense oedometric compression test results. Also, the deviations of β are very high for some input sets. However, no clear correlation between the different input sets and the impact on parameter β could be found.

7. Full KIM analysis

In the next step full KIM analyses were executed. The analyses were performed on the one hand with the hypoplastic parameter "Set 0" given in [6] and on the other hand with hypoplastic parameters obtained from the ExCalibre calibration. For this comparison the input set 4 was taken, (further denoted as "ExCalibre 4" – see Table 6). This parameter set is a result of a calibration using both oedometric compression tests and the triaxial tests of the dense soil sample as input for ExCalibre. Both parameter sets and their deviations to each other can be seen in Table 6. From this follows, that the automatic calibration (with ExCalibre) delivers a very good agreement with the "manually" calibrated parameters given in [6] except the α-value (which shows a difference of approximately 500%). Due to this big deviation of the α-value another full KIM analysis was performed using the calibrated parameters from ExCalibre set 4 in combination with a α-value of 0.05 (reference value of "Set 0"). This parameter set is subsequently denoted as "ExCalibre 4b". Hence, in total full KIM analyses are performed for three different parameter sets.

7.1.1. KIM parameters

The limit pressures p_{LS} obtained from the FEA of the spherical cavity expansions (using the three parameter sets) are used in the nest step to determine the KIM parameters a_1, a_2, a_3, b_1, b_2 and b_3 (see Eq. (7)) by applying the curve fitting procedure developed by Winkler [10]. The obtained values of a_i and b_i for the three hypoplastic parameter sets ("Set 0" according to [6], "ExCalibre 4" and "ExCalibre 4b") are then compared with the "reference" KIM parameters given in [6]. This comparison can be seen in Table 7. The KIM parameters are then used to determine the parameters a and b for different relative densities, and subsequently to calculate the limit pressure for different relative densities and different effective mean pressures (as shown in Eq. (3), (4) and (5)). To evaluate the impact of the inidvidual KIM parameters a_i and b_i the a- and b-values were calculated for different relative densities (shown in Fig. 17).

From Fig. 17 follows that the parameters a and b resulting from the hypoplastic parameter "Set 0" and the "ExCalibre set 4b" (α-value of "Set 0") agree very well with the values given in [6]. For "ExCalibre Set 4" the values of a and b show only a good agreement for low relative densities, whereas for higher relative densities both parameters (a and b) show high deviations with a maximum of around 100%.

The final p_{LS}-p_0' curves for different relative densities I_D using the calculated KIM parameters from the hypoplastic parameter "Set 0" and "ExCalibre set 4" are presented in Fig. 18.

Table 7. Calculated KIM parameters for three different hypoplastic parameter sets and KIM parameters given in [6]

Parameter	KIM Parameters [6]	Set 0	ExCalibre 4	ExCalibre 4b
a_1	1.666	1.622	-1.520	1.294
a_2	-6.152	-5.330	-8.587	-5.139
a_3	-1.597	-1.535	-1.290	-1.429
b_1	0.835	0.829	1.037	0.860
b_2	0.073	0.078	0.302	0.060
b_3	-1.395	-1.459	-1.416	-1.404

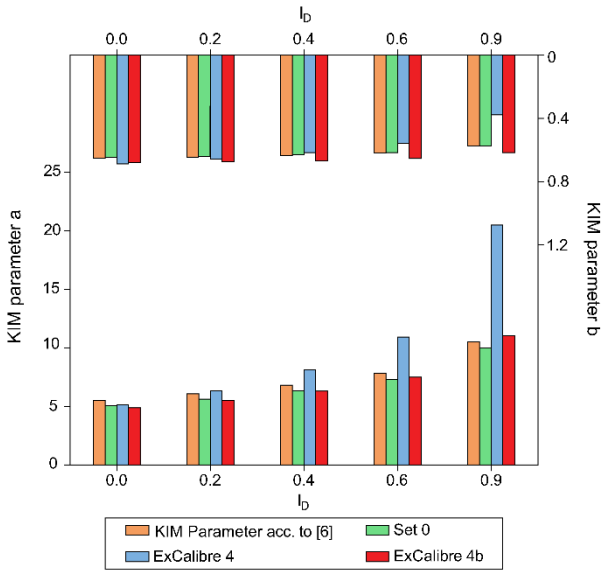

Figure 17. KIM parameter a and b for selected relative densities

The limit pressures denoted as "p_{LS} explicit" are the respective results obtained from the spherical cavity expansion analyses for different relative densities and different mean effective pressures p_0'. Fig. 18 indicates that for lower relative densities both p_{LS} curves are very similar, but for I_D values larger than 0.3, the limit pressures show deviations of over 100%. The resulting curves for the ExCalibre parameter set 4b (with the α-value of "Set 0") show very similar results as p_{LS}-p_0' curves using the hypoplastic parameter "Set 0".

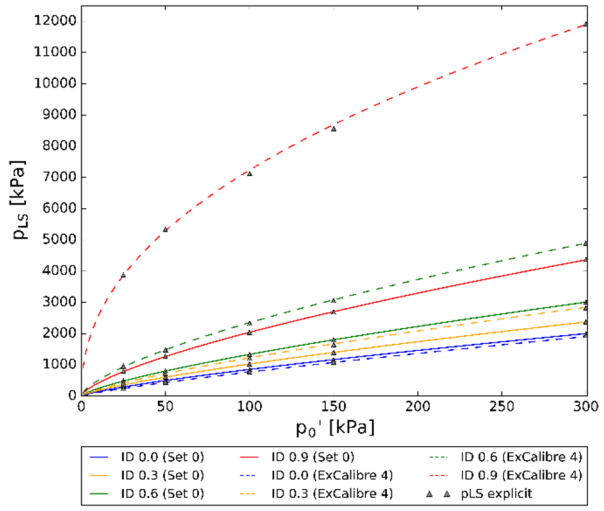

Figure 18. p_{LS}-p_0' curves for "Set 0" [6] and "ExCalibre set 4"

7.1.2. Calculation of q_c

The final aim of the KIM is to provide the correlation between the cone resistance q_c and a certain relative density I_D. Combining the Eq. (1) to (5) the final equation is as follows:

$$q_c = \left(1.5 + \frac{5.8 * {I_D}^2}{{I_D}^2 + 0.11}\right) * \left(a_1 + \frac{a_2}{a_3 + I_D}\right) * p'(z)^{\left(b_1 + \frac{b_2}{b_3 + I_D}\right)} \quad (7)$$

The first part represents the shape factor k_q as defined in Eq. (2) and the effective mean pressure $p'(z)$ can be determined with the effective vertical stress $\sigma_v'(z)$ and the lateral earth pressure coefficient K_0.

$$p'(z) = \frac{1}{3} * \sigma_v'(z) * (1 + 2 * K_0) \quad (8)$$

Because the mean effective pressure $p'(z)$ increases with depth, the calculated void ratios are decreasing with depth (for a certain relative density). The actual void ratio, related to a certain relative density, can be calculated with the limit void ratios e_c and e_d, where the limit void ratios e_c and e_d are pressure-depended. Hence, they have to be determined by using the effective mean pressure $p'(z)$ and the compression law according to Bauer [19] (see Eq. (10)).

$$I_D = \frac{e_c - e(z)}{e_c - e_d} \rightarrow e(z) = e_c - I_D * (e_c - e_d) \quad (9)$$

$$\frac{e_c}{e_{c0}} = \frac{e_d}{e_{d0}} = \frac{e_i}{e_{i0}} = exp\left[-\left(\frac{3p'}{h_s}\right)^n\right] \quad (10)$$

A change of the void ratio in turn also effects the density and subsequently the unit weight of the soil. Thus, a decrease of the void ratios causes an increase of the dry density, as shown below in Eq. (11) and (12).

$$\rho_d(z) = \frac{\rho_s}{1 + e(z)} \quad (11)$$

$$\gamma(z) = (1 + w) * \rho_d(z) * g \quad (12)$$

Where ρ_d is the dry density, ρ_s the grain density and w the assumed water content of the soil. The result of Eq. (12) is then used in the next step to calculate the vertical effective pressure $\sigma_v'(z)$, which is required to determine the mean effective pressure $p'(z)$. And finally, by using Eq. (7), the cone resistance q_c can be calculated for different values of I_D.

In the following, the cone resistances for the relative densities $I_D = 0.1$ and $I_D = 0.3$ are discussed. The results, namely q_c over depth (for all four analyzed material sets) are plotted in Fig. 19.

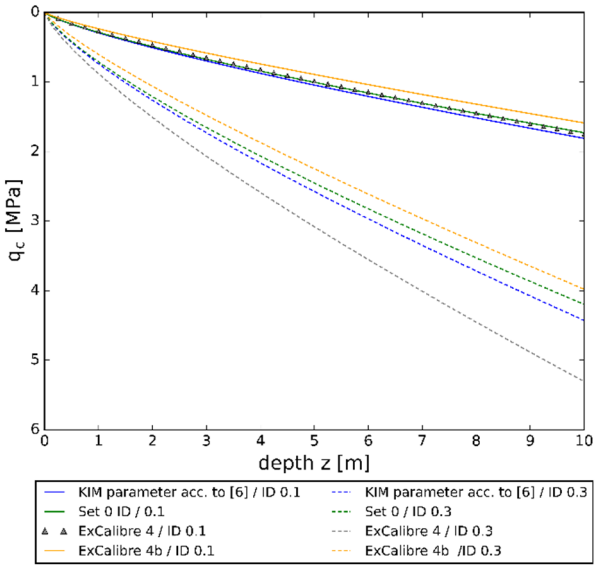

Figure 19. q_c curves for relative density $I_D = 0.1$ and $I_D = 0.3$

Similar conclusions that have been drawn in chapter 7.1.1 can also be concluded from Fig. 19. The cone resistances obtained from the hypoplastic parameter "Set 0" show (as expected) for all investigated relative densities similar results as obtained with the KIM parameters given in [6], whereas the calculated cone resistances for the hypoplastic parameters of the ExCalibre calibration (Set 4) are only similar for low relative densities. With ExCalibre parameter set 4 significant deviations were found for higher I_D-values ($I_D > 0.3$). However, by changing the magnitude of parameter α (Set 4b) the results yield (again) almost similar q_c-curves for all relative densities. These studies indicate the high sensitivity of the KIM to certain input parameters of the hypoplastic soil model.

7.2. Automation of the KIM analysis

Due to the fact that a full KIM analysis is very time consuming the final goal of the performed research is a fully automatized KIM analyzing process. At the moment most of the processes have already been automated using Python. The flowchart shown in Figure 20 gives an overview of the step-by-step procedure up to the calculated correlation between the relative density and the cone resistance.

Initially, the user has to input the hypoplastic parameters to the finite element model and the Python script. Then the script runs 50 finite element analyses with different initial void ratios and different initial stress states. Subsequently, the user obtains the pressure-expansion curves for all considered relative densities and initial stress states and the limit pressures for each of the 50 spherical cavity expansion models. These limit pressures are automatically transferred to an EXCEL worksheet provided by Winkler [10] for the curve fitting procedure. Afterwards, the calculated KIM parameters a_i and b_i as well as the hypoplastic parameters have to be transferred to the Python file, in order to obtain the p_{LS} curves over p_0'. Finally the cone resistances are automatically plotted over the penetration depth for different relative densities.

8. Conclusion

It can be concluded, that the presented finite element model to analyse the spherical cavity expansion problem computes very similar pressure-expansion curves as calculated with the closed-form solution by Yu & Houlsby [13], regardless of the magnitude of the dilatancy angle ψ. However, the studies also showed that an increasing dilatancy angle results in significantly higher limit pressures. The results obtained with the linear elastic-perfectly plastic MC model indicate, that with an increasing dilatancy angle, no horizontal tangent of the pressure expansion curves, hence no well defined limit pressure can be computed. When using more advanced constitutiove models this problem can be controlled by defining a dilatancy-cut-off at a certain maximum void ratio e_{max}. Moreover, it was highlighted that higher lateral earth pressure coefficients lead to higher limit pressures. The presented investigations show additionally, that the application of a uniform initial stress field provides nearly the same results as a non-uniform stress field. Chapter 5 illustrates that the Hardening Soil model is able to compute similar results of the spherical cavity expansion as the hypoplastic soil model. However, using KIM in combination with the HS model is associated with a high effort related to the optimization of the input parameters for the constitutive model, since the HS model does not take pyknotropy into account. With respect to the Karlsruhe Interpretation Method and the automatic hypoplastic parameter calibration tool ExCalibre, it is shown, that ExCalibre is a very helpful tool to determine the input parameters for the hypoplastic soil model. However, based on the investigations it turned out that the number and the type of laboratory tests (provided to the ExCalibre input file) has a significant influence on the resulting hypoplastic parameters. It was also found that most of the input parameters optimized by means of ExCalibre show a very good agreement with the "experience-based" parameter determination of the hypoplastic model. However, the performed studies showed a significant deviation between "classical" parameter determination and ExCalibre for the input paramter α, which controls the material's peak friction angle and hence the dilatancy behaviour of the material.

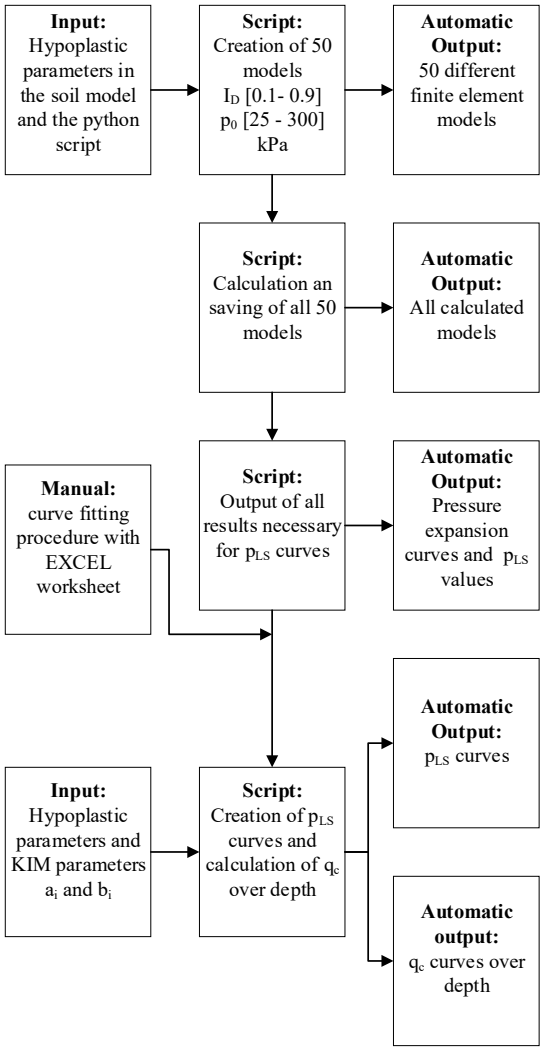

Figure 20. Flowchart of full KIM analysis process

Finally the automation of the entire KIM analysis is briefly discribed. It is shown that with the utilization of the remote scripting tool of PLAXIS the analysis can be performed almost fully automatic. This development increases on the one hand the user friendliness of the KIM and contributes on the other hand to speed up the calculation time of such time-consuming investigations.

Further studies regarding the verfication of the KIM are (at the moment) in progress, focusing on the comparison of the KIM with the Press-Replace Method [20]. Additionally it is believed, that the performance of the KIM for calcarous sands can be improved by taking grain crushing effects into account. Therefore, research is currently performed using a hypoplastic model for crushable sand [21], which requires, compared to the hypoplastic soil model according to Von Wolffersdorff [8], only two additional physical parameters, namely the uniformity coefficient C_u and the mean grain size d_{50}.

9. References

[1] Schmertmann, J. H., "An Updated Correlation Between Relative Density Dr and Fugro-Type Electric Cone Bearing, qc", Contract Report DACW 39-76 M 6646 WES, Wicksburg, Mississippi, Technical Report, 19676

[2] Baldi, G., Bellotti, R., Ghionna, N., Jamiolkowski, M., Pasqualini, E. "Interpretation of CPTs and CPTUs, 2nd part: drained penetration of sands", In: 4th International Geo-technical Seminar, Field Instrumentation and In-Situ Measurements, 1986, pp. 143 – 155.

[3] Tschuchnigg, F., Reinisch, J., Thurner, R. "Estimation of the relative Density in Calcareous Sands using the Karlsruhe Interpretation Method", In: Wu W., Yu HS. (eds) Proceedings of China-Europe Conference on Geotechnical Engineering, Springer Series in Geomechanics and Geoengineering, Springer, Cham, 2018. https://doi.org/10.1007/978-3-319-97112-4_164

[4] Tschuchnigg, F., Winkler, M. B. "KIM – Numerical studies on the spherical cavity expansion problem", European Conference on Soil Mechanics and Geotechnical Engineering, Reykjavik, Iceland, Sept., 1-6, 2019

[5] Gudehus, G., Amorosi, A., Gens, A., Herle, I., Kolymbas, D., Mašín, D., Muir Wood, D., Nova, R., Niemunis, A., Pastor, M., Tamagnini, C. and Viggiani, G. "The soilmodels.info project", In: International Journal for Numerical and Analytical Methods in Geomechanics, 32(12), pp. 1571-1572, 2008. https://doi.org/10.1002/nag.675

[6] Thurner, R., Reinisch, J., Tschuchnigg, F. "Influence of the Carbonate Content on CPT-Results and Practical Relevance for the Soil Improvement Works on Major Land Reclamation Projects", In: Shehata H., Poulos H. (eds) Latest Thoughts on Ground Improvement Techniques, GeoMEast 2018, Sustainable Civil Infrastructures, Springer, Cham, (2019). https://doi.org/10.1007/978-3-030-01917-4_10

[7] Cudmani, R. "Statische, alternierende und dynamische Penetration in nichtbindigen Böden", PhD thesis, University Fridericiana Karlsruhe, 2000.

[8] Von Wolffersdorff, P. "A hypoplastic relation for granular materials with a predefined limit state surface", Mechanics of Cohesive-Frictional Materials, 1, pp. 251 – 271, 1996. https://doi.org/10.1002/(SICI)1099-1484(199607)1:3<251::AID-CFM13>3.0.CO;2-3

[9] Meier, T. "Application of Hypoplastic and Viscohypoplastic Constitutive Models for Geotechnical Problems", PhD Thesis, University Fridericiana Karlsruhe, 2007.

[10] Winkler, M. B. "KIM – Investigation of spherical cavity expansion employing different constitutive models", Master's thesis, Technical University of Graz, 2018.

[11] Cudmani, R., Osinov, V. A. "The cavity expansion problem for the interpretation of cone penetration and pressuremeter tests", Canadian Geotechnical Journal, 38, pp. 622 – 638, 2001. https://doi.org/10.1139/t00-124

[12] Brinkgreve, R. B. J., Kumarswamy, S., Swolfs, W. M., Zampich, L., Ragi Manoj, N. "PLAXIS 2018. Finite element code for soil and rock analyses, User Manual". Delft: Plaxis bv.

[13] Yu, H. S., Houlsby, G. "Finite cavity expansion in dilatant soils: loading analysis", Geotechnique, 41(2), pp. 173 – 183, 1991.

[14] Schanz, T., Vermeer, P. A., Bonnier, P. G. "The hardening soil model: Formulation and verification", In: Beyond 2000 in Computational Geotechnics (eds.) Brinkgreve, Balkema, Rotterdam, 1999, pp. 281 – 296.

[15] Jaky, J. "Pressures in silos", In: Proceedings of the 2nd International Conference in Soil Mechanics and Foundation Engineering, Rotterdam, Netherlands, 1948, pp. 103-107.

[16] Tschuchnigg, F. "3D Finite Element Modelling of Deep Foundations Employing an Embedded Pile Formulation", PhD thesis, Technical University of Graz, 2012

[17] Xu, X. "Investigation of the End Bearing Performance of Displacement Piles in Sand", PhD thesis, University of Western Australia, 2007.

[18] Marcher, T., Vermeer, P. A., Von Wolfersdorff, P. A. "Hypoplastic and elastoplastic modelling – a comparison with test data", In: Kolymbas D. (eds) Constitutive Modelling of Granular Materials, Springer, Berlin, Germany, 2000, pp: 353 - 374. https://doi.org/10.1007/978-3-642-57018-6_17

[19] Bauer, E. "Calibration of a Comprehensive Hypoplastic Model for Granular Materials", Soils and Foundations, 36(1), pp. 13-26,1996.

[20] Xian, L. Y. "Numerical Study of Cone Penetration Test in Clays using Press-Replace Method", PhD Thesis, National University of Singapore, 2017.

[21] Phuong, N. T. V., Rohe, A., Brinkgreve, R. B. J., van Tol, A. F. "Hypoplastic model for crushable sand", Soils and Foundations, 58(3), pp. 615-626, 2018. https://doi.org/10.1016/j.sandf.2018.02.022